Received: 13 June 2023 | Accepted: 15 June 2023

DOI: 10.1002/ajh.27013

RESEARCH ARTICLE

Clonal dynamics and copy number variants by single-cell analysis in leukemic evolution of myeloproliferative neoplasms

Laura Calabresi[1,2] | Chiara Carretta[3,4] | Simone Romagnoli[1,2] | Giada Rotunno[1,2] | Sandra Parenti[3,4] | Matteo Bertesi[3,5] | Niccolò Bartalucci[1,2] | Sebastiano Rontauroli[3,4] | Chiara Chiereghin[6] | Sara Castellano[3,4] | Giulia Gentili[1,2] | Chiara Maccari[1,2] | Fiorenza Vanderwert[1,2] | Francesco Mannelli[1,2] | Matteo Della Porta[6] | Rossella Manfredini[3,4] | Alessandro Maria Vannucchi[1,2] | Paola Guglielmelli[1,2]

[1]Center Research and Innovation of Myeloproliferative Neoplasms (CRIMM), Azienda Ospedaliera-Universitaria Careggi, Florence, Italy

[2]Department of Experimental and Clinical Medicine, University of Florence, Florence, Italy

[3]Centre for Regenerative Medicine "S. Ferrari", University of Modena and Reggio Emilia, Modena, Italy

[4]Department of Biomedical, Metabolic and Neural Sciences, University of Modena and Reggio Emilia, Modena, Italy

[5]Department of Life Sciences, University of Modena and Reggio Emilia, Modena, Italy

[6]Humanitas Clinical and Research Center-IRCCS, Rozzano, Milan, Italy

Correspondence
Alessandro Maria Vannucchi, Department of Experimental and Clinical Medicine, University of Florence, CRIMM, Azienda Ospedaliero-Universitaria Careggi, Viale Pieraccini 6, pad 27B, 50139 Florence, Italy.
Email: amvannucchi@unifi.it

Funding information
Associazione Italiana Ricerca sul cancro, Grant/Award Number: 1267; Cancer Research UK, Fondazione AIRC and Fundación Científica de la Asociacion Española Contra el Cáncer; Italian Ministry of Health

Abstract

Transformation from chronic (CP) to blast phase (BP) in myeloproliferative neoplasm (MPN) remains poorly characterized, and no specific mutation pattern has been highlighted. BP-MPN represents an unmet need, due to its refractoriness to treatment and dismal outcome. Taking advantage of the granularity provided by single-cell sequencing (SCS), we analyzed paired samples of CP and BP in 10 patients to map clonal trajectories and interrogate target copy number variants (CNVs). Already at diagnosis, MPN present as oligoclonal diseases with varying ratio of mutated and wild-type cells, including cases where normal hematopoiesis was entirely surmised by mutated clones. BP originated from increasing clonal complexity, either on top or independent of a driver mutation, through acquisition of novel mutations as well as accumulation of clones harboring multiple mutations, that were detected at CP by SCS but were missed by bulk sequencing. There were progressive copy-number imbalances from CP to BP, that configured distinct clonal profiles and identified recurrences in genes including *NF1*, *TET2*, and *BCOR*, suggesting an additional level of complexity and contribution to leukemic transformation. *EZH2* emerged as the gene most frequently affected by single nucleotide and CNVs, that might result in EZH2/PRC2-mediated transcriptional deregulation, as supported by combined scATAC-seq and snRNA-seq analysis of the leukemic clone in a representative case. Overall, findings provided insights into the pathogenesis of MPN-BP, identified CNVs as a hitherto poorly characterized mechanism and point to EZH2 dysregulation as

Laura Calabresi and Chiara Carretta contributed equally to this study.

Rossella Manfredini, Alessandro Maria Vannucchi, and Paola Guglielmelli are senior authors.

target. Serial assessment of clonal dynamics might potentially allow early detection of impending disease transformation, with therapeutic implications.

1 | INTRODUCTION

Myeloproliferative neoplasms (MPN) are characterized by the expansion of one or more myeloid cell lineages and include four entities: polycythemia vera (PV), essential thrombocythemia (ET), overt and prefibrotic primary myelofibrosis (PMF).[1,2] In addition to the *JAK2*, *CALR*, and *MPL* driver mutations, MPN are characterized by remarkable genetic heterogeneity with mutations in genes coding for epigenetic and spliceosome regulators, oncogenes, signaling and transcription factors, that may affect the same or different clones.[3–6]

MPN evolve from chronic (CP) to blast phase (BP) in 5%–10% of cases overall, with highest frequency in PMF (15%–20%), and may be preceded by an accelerated phase (AP).[7,8] MPN-BP is associated with dismal outcome; median survival is 3–6 months.[9] Treatment ranges from supportive care to low-intensity approaches, including hypomethylating agents or low-dose cytarabine, to intensive strategies with induction chemotherapy and allogeneic stem cell transplantation in a minority of younger, fit patients. Complete remission (CR) occurs in <30% of patients.[10–12] Such unfavorable prognosis is consistent with specific features, including advanced age and associated comorbidities that prevent aggressive treatment. Previous studies indicated that the genetic basis of MPN-BP differs from de novo AML: *NPM1* and *FLT3* mutations are uncommon while other abnormalities, such as *IDH1* and *TP53* mutations and complex karyotype, are conversely enriched, possibly reflecting accumulation of mutations and clonal evolution in a decade-lasting disease.[13–16] Two distinct trajectories of clonal evolution to BP have been highlighted.[17,18] In one, leukemic blasts are *JAK2/CALR/MPL* mutated, reflecting acquisition of leukemia-promoting abnormalities in the original CP clone, such as *TP53* mutation and deletion and/or abnormalities of chromosome 1 long arm.[16,19] Otherwise, leukemic blasts derive from a driver mutation-negative clone and eventually overcome the *JAK2/CALR/MPL*^{mut} CP clone.[8,20] MPN-BP blasts often display skewing of erythroid or megakaryocytic lineage phenotype, uncommon in de novo AML,[13] consistent with findings in chronic phase progenitors[21] However, full understanding of mutation and clone dynamics in the progression to MPN-BP has been prevented by methodological constraints, since the heterogeneity of leukemic blasts cannot be fully resolved by conventional bulk sequencing.[22,23]

Herein, we adopted a single-cell approach to study the clonal architecture of CD34$^+$ cells in longitudinal samples of CP and BP from 10 MPN patients, and described models of stepwise acquisition of somatic mutations, clonal dominance and copy number imbalances in the transition to MPN-BP. Moreover, in a representative case, we employed single-cell multiomic approach coupling RNA-seq and ATAC (Assay for Transposase-Accessible Chromatin)-seq to concurrently analyze transcriptomic and epigenetic changes during leukemic transformation.

2 | PATIENTS AND METHODS

We analyzed 10 MPN patients who developed BP (T2) and had available paired samples collected at CP diagnosis (T0) (Tables S1 and S2 for clinical and molecular information). After approval by the Institutional Review Board (IRB) in Florence and Milan (Italy), written informed consent was obtained according to the Declaration of Helsinki.

2.1 | NGS analysis on bulk samples

Procedure details and list of genes included in bulk next generation sequencing (NGS) panels are reported in Supplemental Methods.

2.2 | Single-cell (SC) targeted DNA library preparation and sequencing

Immunomagnetically purified, blood-derived, CD34$^+$ cells were used for generation of single-cell DNA libraries according to Tapestri platform standard protocol. Libraries were sequenced on Illumina NovaSeq. All samples were subjected to 2 × 150 bp paired-end sequencing, with the exception of *CALR*-mutated samples, which underwent 2 × 250 bp paired-end sequencing. Full procedure and bioinformatic pipeline details are reported in Supplemental Methods.

2.3 | Combined single cell assay for transposase-accessible chromatin sequencing (scATACseq) and single nucleus RNA-seq (snRNA-seq) library preparation

Nuclei were isolated from CD34$^+$ cells after resuspension in lysis buffer containing 0.01% Digitonin; 6000 nuclei per sample were loaded onto 10× cartridge, in the presence of 1 U/μL RNase inhibitor. Libraries were sequenced on Illumina NextSeq 550 using 2 × 75 bp paired-end sequencing.

2.4 | Statistical analysis

Statistical significance was evaluated using Wilcoxon sum rank test and Benjamini–Hochberg/FDR test for multiple test correction. For

co-occurrence analysis, the maftools package in R was used. Clustering was performed using the Mosaic's module dna.count using min_clone_size (the minimum proportion of cells in the clone necessary to count it as a separate clone), parameter set to 0.5. Details of the analysis to determine SC ploidy changes can be found at https://github.com/littleisland8/TACOS.

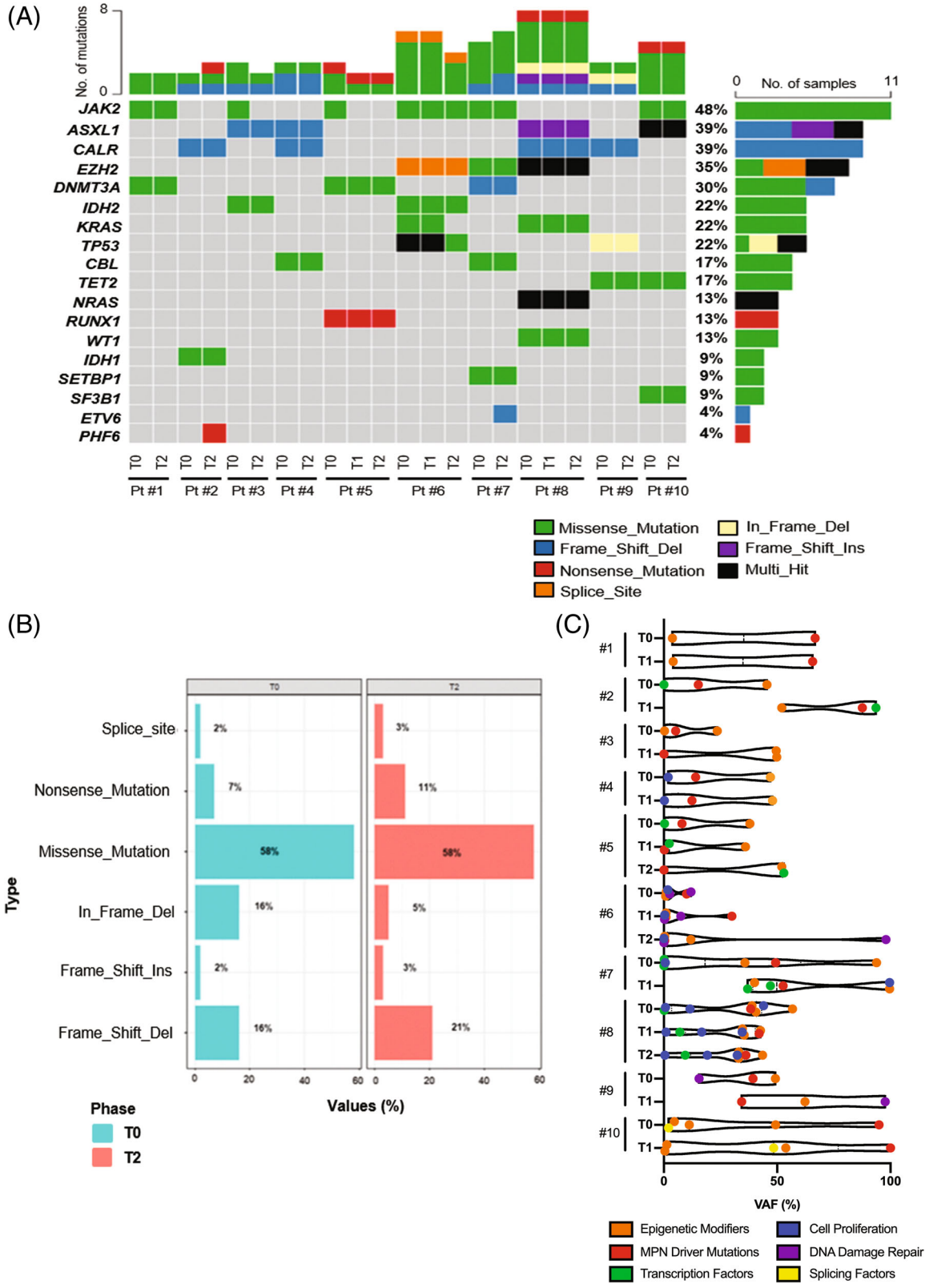

FIGURE 1 Legend on next page.

3 | RESULTS

3.1 | Single-cell DNA sequencing (SCS) detects additional subclonal mutations compared to bulk sequencing

To characterize the clonal architecture of the stem cell compartment at diagnosis and leukemic transformation, we performed SCS using either a 312-amplicons or a 239-amplicons custom panel in 7 and 3 patients, respectively, covering 45 and 29 of the most frequently mutated genes in myeloid neoplasms (Figure S1A,B and Tables S3 and S4). We analyzed paired samples from 10 patients at diagnosis (T0) and blast phase (T2); an additional sample (T1) collected at diagnosis of postPV-MF transformation (PPV-MF, #6), accelerated phase (AP, #8) or attribution of *JAK2*pV617F major molecular response (#5),[14] was also analyzed in 3 cases. A total of 104 072 individual cells (average 4525, range 1645-8476, per sample) was sequenced; median sequencing coverage was 118 reads per amplicon per cell, and the calculated median allele dropout (ADO) rate was 7.15% to 21.5% per sample, overall 11.4% (Figure S1C). By comparing results of SCS and bulk sequencing, we found that all variants called by bulk NGS were confirmed by SCS, and the respective variant allele fractions (VAF) were significantly correlated ($R^2 = 0.85$, Pearson correlation) (Figure S1D); however, SCS was able to detect 17 additional low-frequency variants (VAF < 2%), particularly at T0, that in several cases increased significantly at BP.

3.2 | Resolution of clonal architecture at chronic and blast phase

Overall, a total of 41 coding somatic mutations in 18 genes were identified by SCS in the 10 patients. *JAK2*p.V617F was the most frequent (48%), followed by *ASXL1*^{mut} (39%), *CALR* ^{mut} (39%) and *EZH2*^{mut} (35%) (Figure 1A). Frequency of missense mutations was similar at T0 and T2 (58%) (Figure 1B), while frameshift deletions tended to increase in T2 (21% vs. 16%) and in-frame deletions to decrease (5% vs. 16%). Almost half of all mutations at BP involved epigenetic genes (*ASXL1*, *TET2*, *EZH2*, *IDH1*, *DNMT3A*). Analysis of mutation co-occurrence and mutual exclusivity revealed that most frequently co-occurring mutations in ≥2 clones included *TP53/TET2*, *DNMT3A/JAK2*, *RUNX1/DNMT3A* and *NRAS/EZH2*, while *DNMT3A* and *ASXL1* were mutually exclusive ($p < .05$ for all combinations). We also observed that *TP53*^{mut} frequently occurred in clones not harboring *JAK2*p.V617F or *ASXL1*^{mut} ($p < .05$) (Figure S2). Finally, we noticed that the VAF of mutated transcription factor genes (*ETV6*, *PHF6*, *RUNX1*, *WT1*, *SETBP1*) was remarkably increased compared to CP (Figure 1C).

We were able to longitudinally investigate the clonal architecture in all but 2 patients (#1 and #4), since in both cases the mutation dominating the BP, as highlighted by bulk NGS, was not covered by SCS panel (Figure S3). In one, a *KRAS*p.A146T increased from 9% at T0 to 47% at T2; in the other, a *IKZF1*p.R502W increased from 4.4% to 40.7% (Table S2). In the remaining 8 patients, in spite of intra- and inter-patient heterogeneity, we were able to recognize some unique clonal patterns and trajectories that helped to identify the clone(s) ultimately dominating the BP (Figure 2).

A first pattern included patients in which no wild-type CD34$^+$ cells could be demonstrated at diagnosis (Figure 2A,B). In patient #8, a *CALR*-type1^{mut} PMF, an additional sample collected at AP (T1) was analyzed. At T0 he carried 3 branches that, by clonal phylogeny reconstruction, were ascribed to a *ASXL1*p.G646Wfs*12 founder clone that however could not be physically identified. The first branch, accounting for 2/3 of CD34$^+$ cells, carried 2 distinct heterozygous *EZH2*^{mut}, a *NRAS*p.G12V^{mut}, and subsequently acquired *CALR*^{mut}. A second branch acquired a *NRAS*p.G12S ^{mut} and an *EZH2* indel, followed by *CALR*^{mut}; these 2 subclones, that were 30% at CP, dramatically decreased at AP and BP (2% and 3% respectively). In the third evolutionary branch, *KRAS*p.G12D^{mut} was acquired on top of *ASXL1*^{mut}, followed by *CALR*^{mut} and *WT1*p.R467W^{mut} in 2 independent subclones. Overall, this evolutionary branch was <2% at CP and increased to 31% at AP and 40% at BP, therefore representing the leukemia-driving clone. Noteworthy, at CP, the *KRAS*^{mut} and *WT1*^{mut} were missed by bulk NGS unlike by SCS (VAF 0.7% and 0.1%, respectively). A second case (#9, Figure 2B) was a *CALR*-type1^{mut} ET. Clonal phylogeny reconstruction identified *TET2*p.D1384G as the first occurring mutation (41% at diagnosis) that subclonally associated with *CALR*^{mut} (45%) or heterozygous *TP53*p.G244_M246del (12%); a minor *TET2/TP53/CALR*^{mut} clone was also detected (1.2%). Evolution to BP was triggered by selective expansion of heterozygous *TET2*^{mut}/

FIGURE 1 Mutational profiling landscape as highlighted by SCS. (A) Oncoplot showing mutation profiles of each gene in each sample. The barplot on the right shows the gene ordered by mutation frequency, listed on the left. (B) Frequency of different mutation classes in T0 and T2. (C) Violin plot depicting single cell allele frequency of mutations classified according to the molecular function of the affected genes. Each violin displays the mutational landscape of an analyzed timepoint. Violins are grouped by patient ID. Genes were classified as follows: Epigenetic Modifiers (*ASXL1*, *EZH2*, *TET2*, *IDH1*, *IDH2*, *DNMT3A*), MPN Driver Mutations (*JAK2*, *CALR*), Transcription Factors (*PHF6*, *RUNX1*, *ETV6*, *WT1*, *SETBP1*), DNA Damage Repair (*TP53*), Cell Proliferation (*NRAS*, *KRAS*, *CBL*), Splicing Factors (*SF3B1*). *ASXL1*, Additional Sex Combs Like Transcriptional Regulator 1; *CBL*, Cbl Proto-Oncogene; *CALR*, Calreticulin; DEL, deletion; *DNMT3A*, DNA Methyltransferase 3 α; *EZH2*, Additional Sex Combs Like 1, Transcriptional Regulator; *ETV6*, ETS Variant Transcription Factor 6; INS, insertion; *IDH1/2*, Isocitrate Dehydrogenases 1/2; *JAK2*, Janus Kinase 2; *KRAS* Kirsten Rat Sarcoma Viral Oncogene Homolog; *NRAS*, Neuroblastoma RAS Viral Oncogene Homolog; *PHF6*, PHD Finger Protein 6; *RUNX1*, Runt-related transcription factor 1; *SETBP1*, SET binding protein 1; *SF3B1*, Splicing factor 3B subunit 1; SNP, single nucleotide polymorphism; SNV, single nucleotide variants; *TET2*, Ten-Eleven-Translocation 2; *TP53*, Tumor Protein 53; *WT1*, Wilms Tumor 1.

homozygous *TP53*^{mut} clone, that increased from <3% at CP to 83% at BP. A double homozygous *TET2*^{mut}/*TP53*^{mut} clone, not detected at CP, also contributed to BP (16%).

A second pattern (PMF patients #7, #2; Figure 2C,D) showed stepwise clonal progression starting, respectively, from founder homozygous *EZH2*p.F551V or heterozygous *IDH1*p.R132H clone. In

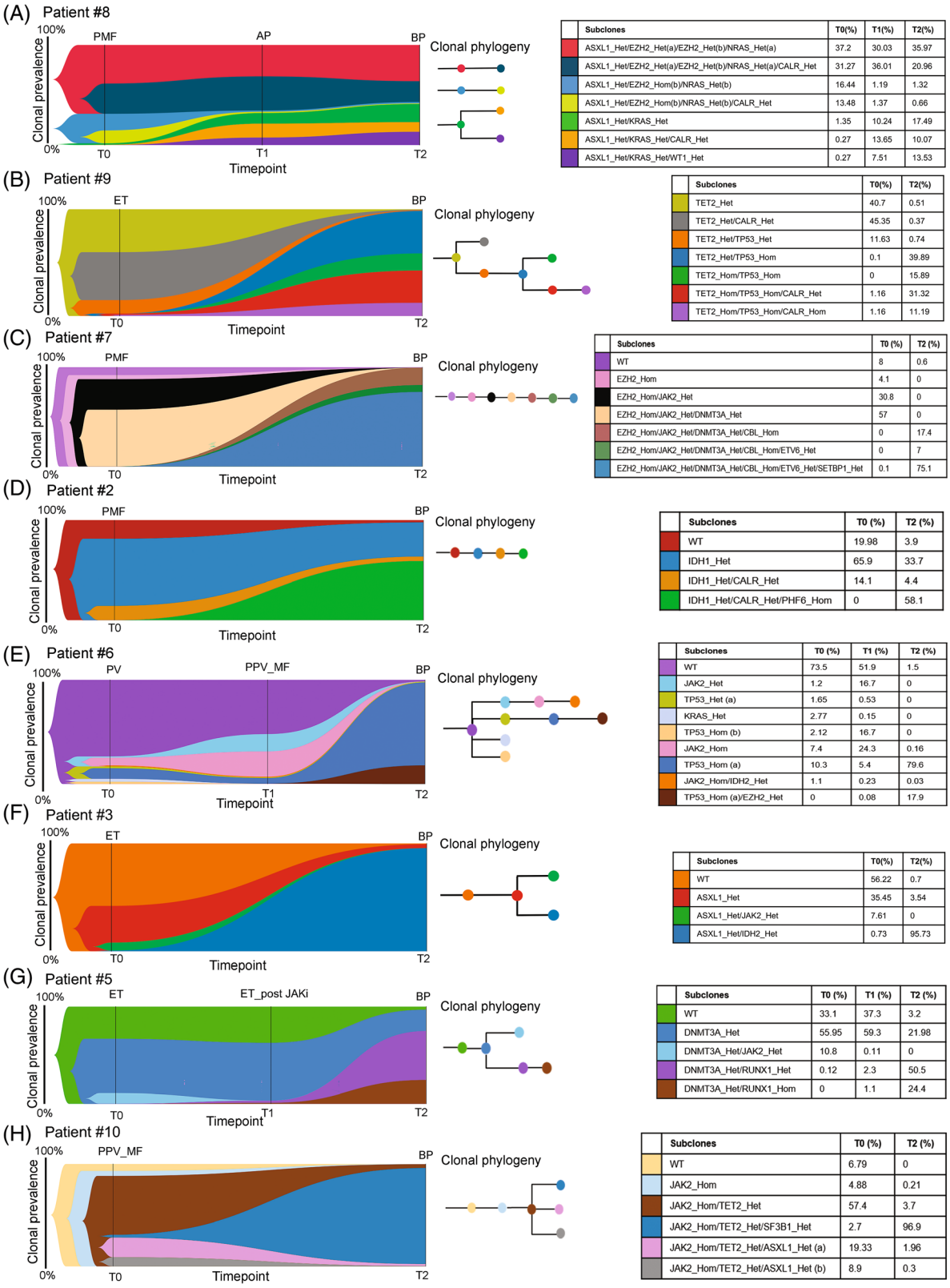

Subclones	T0(%)	T1(%)	T2(%)
ASXL1_Het/EZH2_Het(a)/EZH2_Het(b)/NRAS_Het(a)	37.2	30.03	35.97
ASXL1_Het/EZH2_Het(a)/EZH2_Het(b)/NRAS_Het(a)/CALR_Het	31.27	36.01	20.96
ASXL1_Het/EZH2_Hom(b)/NRAS_Het(b)	16.44	1.19	1.32
ASXL1_Het/EZH2_Hom(b)/NRAS_Het(b)/CALR_Het	13.48	1.37	0.66
ASXL1_Het/KRAS_Het	1.35	10.24	17.49
ASXL1_Het/KRAS_Het/CALR_Het	0.27	13.65	10.07
ASXL1_Het/KRAS_Het/WT1_Het	0.27	7.51	13.53

Subclones	T0(%)	T2(%)
TET2_Het	40.7	0.51
TET2_Het/CALR_Het	45.35	0.37
TET2_Het/TP53_Het	11.63	0.74
TET2_Het/TP53_Hom	0.1	39.89
TET2_Hom/TP53_Hom	0	15.89
TET2_Hom/TP53_Hom/CALR_Het	1.16	31.32
TET2_Hom/TP53_Hom/CALR_Hom	1.16	11.19

Subclones	T0 (%)	T2 (%)
WT	8	0.6
EZH2_Hom	4.1	0
EZH2_Hom/JAK2_Het	30.8	0
EZH2_Hom/JAK2_Het/DNMT3A_Het	57	0
EZH2_Hom/JAK2_Het/DNMT3A_Het/CBL_Hom	0	17.4
EZH2_Hom/JAK2_Het/DNMT3A_Het/CBL_Hom/ETV6_Het	0	7
EZH2_Hom/JAK2_Het/DNMT3A_Het/CBL_Hom/ETV6_Het/SETBP1_Het	0.1	75.1

Subclones	T0 (%)	T2 (%)
WT	19.98	3.9
IDH1_Het	65.9	33.7
IDH1_Het/CALR_Het	14.1	4.4
IDH1_Het/CALR_Het/PHF6_Hom	0	58.1

Subclones	T0 (%)	T1 (%)	T2 (%)
WT	73.5	51.9	1.5
JAK2_Het	1.2	16.7	0
TP53_Het (a)	1.65	0.53	0
KRAS_Het	2.77	0.15	0
TP53_Hom (b)	2.12	16.7	0
JAK2_Hom	7.4	24.3	0.16
TP53_Hom (a)	10.3	5.4	79.6
JAK2_Hom/IDH2_Het	1.1	0.23	0.03
TP53_Hom (a)/EZH2_Het	0	0.08	17.9

Subclones	T0(%)	T2(%)
WT	56.22	0.7
ASXL1_Het	35.45	3.54
ASXL1_Het/JAK2_Het	7.61	0
ASXL1_Het/IDH2_Het	0.73	95.73

Subclones	T0 (%)	T1 (%)	T2 (%)
WT	33.1	37.3	3.2
DNMT3A_Het	55.95	59.3	21.98
DNMT3A_Het/JAK2_Het	10.8	0.11	0
DNMT3A_Het/RUNX1_Het	0.12	2.3	50.5
DNMT3A_Het/RUNX1_Hom	0	1.1	24.4

Subclones	T0 (%)	T2 (%)
WT	6.79	0
JAK2_Hom	4.88	0.21
JAK2_Hom/TET2_Het	57.4	3.7
JAK2_Hom/TET2_Het/SF3B1_Het	2.7	96.9
JAK2_Hom/TET2_Het/ASXL1_Het (a)	19.33	1.96
JAK2_Hom/TET2_Het/ASXL1_Het (b)	8.9	0.3

FIGURE 2 Legend on next page.

patient #7, heterozygous *JAK2*p.V617F, *DNMT3A*^{mut}, *CBL*^{mut} and *ETV6*^{mut} accumulated stepwise in the founder *EZH2*^{mut} clone. At BP, 75.1% of cells furtherly acquired heterozygous *SETBP1*p.D868N. In patients #2, *CALR*^{mut} was acquired in 14.1% of cells of the founder *IDH1*^{mut} clone (66% at T0); this clone then acquired a homozygous *PHF6*p.Y301*, becoming predominant at BP (58%).

A third pattern regarded the origin of BP clone(s) relative to driver mutation. We found that in 5/8 informative patients, the clone driving the BP arose on the background of driver mutation (*JAK2*p.V617F $n = 2$, *CALR* $n = 3$), unlike 3 *JAK2*p.V617F patients (#6, #3, #5) where the BP was dominated by driver mutation-negative clone(s). In patient #6 (PV), who also had a T1 sample at diagnosis of PPV-MF, clonal phylogeny identified four branches at T0, with WT cells being the majority (73.5%) (Figure 2E). The first branch, made up of 3 subclones at T0 and T1, included cells with heterozygous *JAK2*p.V617F, homozygous *JAK2*p.V617F and homozygous *JAK2*p.V617F plus heterozygous *IDH2*p.R140Q. The second branch included clones harboring heterozygous and homozygous *TP53*p.R136H that were respectively 1.6% and 10.3% at CP; the homozygous *TP53*p.R136H alone or with heterozygous *EZH2*c.1546+2T>C expanded up to 80% and 18%, respectively, at BP. The last two branches at CP (<3% each), including cells with heterozygous *KRAS*p.A59G or homozygous *TP53*p.V134L, were undetected at BP. In the T1 sample, an expansion of heterozygous (from 1.2% to 16.7%) and homozygous (from 7.4% to 24.3%) *JAK2*p.V617F clones was observed, followed by their disappearance at BP. Another case of driver mutation-negative BP was patient #3 (Figure 2F), a *JAK2*p.V617F ET. The first hit affected *ASXL1*p.L775* in 35% of cells, and a subclone (7.6%) acquired *JAK2*p.V617F. The *JAK2*-^{mut} subclone completely disappeared at BP, that was rather dominated (95.7%) by a *ASXL1*p.L775* derivative subclone that acquired *IDH2*p.-R140Q. Of note, the *IDH2*p.R140Q was detected at T0 by SCS in a tiny proportion (0.73%) of cells that was missed by bulk NGS. Finally, in patient #5 (Figure 2G), a *JAK2*p.V617F ET, clonal phylogeny reconstruction identified *DNMT3A*p.G543C as the first hit, followed by splitting into two branches. In one, heterozygous *JAK2*p.V617F was detected in 11% of cells at CP and reduced by 2log (VAF 0.11%) in an intermediate time point sample (T1), in accordance with results of digital PCR that allowed to declare achievement of partial molecular response after 4 years of ruxolitinib. The second branch contained either a heterozygous or homozygous *RUNX1*p.R320X; these clones, that were <5% at T0 and T1, underwent expansion at BP summing up to 75%.

Finally, we identified 2 main patterns regarding the clonal architecture of BP. In 4 of 8 informative patients, multiple clones were found at BP, some of which already detected at CP and others newly emergent (patient #2, 5, 8, 9). In the other four patients, BP was massively dominated by a single clone (>90%) (patient #6, 7, 10, 3) that had expanded from a VAF at CP of <1% (#7, #3) to <10% (#6). This is best exemplified by patient #10 (Figure 2H), a *JAK2*p.V617F PPV-MF. At diagnosis, 93% of the cells presented homozygous *JAK2*p.V617F and acquired a heterozygous *TET2*p.I873T. The latter clone split into 3 branches. The first carried a heterozygous *SF3B1*p.K700E that from 2.7% at CP became dominant at BP (97%). Conversely, the second and third branch, that acquired each a *ASXL1*^{mut} (p.E635Rfs*15 and p.Q858*) and constituted 28% of CP cells, both were no longer detected at leukemic transformation.

3.3 | Accumulation of CNV at blast phase are detected at single cell resolution

We then investigated the occurrence of copy number variation (CNV) events at the SC level by analyzing the ploidy of each amplicon included in the panels. As reference, wild-type cells were used (normalized ploidy value = 2). For patients #8 and #9, in which a wild-type clone could not be detected, the *ASXL1*_Het/*EZH2*_Hom(b)/*NRAS*_Het(b) and *TET2*_Het clones, respectively, were used (see Supplemental Methods for details).

Globally, CNV analysis indicated that leukemic clones were widely affected by gene dosage imbalances, suggesting increased genomic instability compared to CP (Figure 3). The total number of CNVs varied greatly among patients, and several amplicons belonging to the same gene were concurrently involved, supporting large-scale genomic imbalances. In BP clones, we found a total of 434 CNVs, including both copy number gain (41%) and loss (59%), compared to 283 total CNVs in the CP, of which 57% gains and 43% loss. The median number of CNVs per patient in BP clones was 93, ranging from 18 to 158, compared to 13 (0–134) at CP ($p = .04$).

We then compared the ploidy level of individual amplicons in BP versus CP through TACOS algorithm in order to identify any recurrent CNVs. The heatmaps of the clone-to-clone distances shown in Figure S4 illustrate the hierarchical clustering for each patient, indicating the presence of two clusters composed of CP and BP clones, respectively. The heatmaps in Figure 4 depict the significantly

FIGURE 2 Clonal evolution from MPN to sAML. Clonal hierarchy reconstruction by means of fishplot (left) and phylogenetic tree (right). The fish plot shows the inferred clonal evolution pattern based on the single-cell genotype data. Each clone is represented by a different color and the mutation asset is detailed in the legend near the phylogenetic tree with the frequency of the various subclones at different timepoints. (A) Pt #8 carried the *CALR* p.L367Tfs*46 driver mutation. The three depicted timepoints are PMF (T0), AP (T1) and BP (T2). (B) Pt #9 was affected by *CALR* p. L367Tfs*46 driver mutation. The two depicted timepoints are ET (T0) and BP (T2). (C) Pt #7 was affected by *JAK2* p.V617F mutated PMF. The two depicted timepoints are PMF (T0) and BP (T2). (D) Pt#2 carried the *CALR* p.L367Tfs*46 driver mutation. The two depicted timepoints are PMF (T0) and BP (T2). (E) Pt #6 was affected by *JAK2* pV617F driver mutation. The three depicted timepoints are PV (T0), PPV-MF (T1) and BP(T2). (F) Pt #3 was affected by *JAK2* p.V617F driver mutation. The two depicted timepoints are ET (T0) and BP (T2). (G) Pt #5 was affected by *JAK2* p.V617F driver mutation. The three depicted timepoints are ET (T0), ET-post JAKi (T1) and BP (T2). (H) Pt #10 was affected by *JAK2* p.V617F driver mutation. The two depicted timepoints are PPV-MF (T0) and BP (T2).

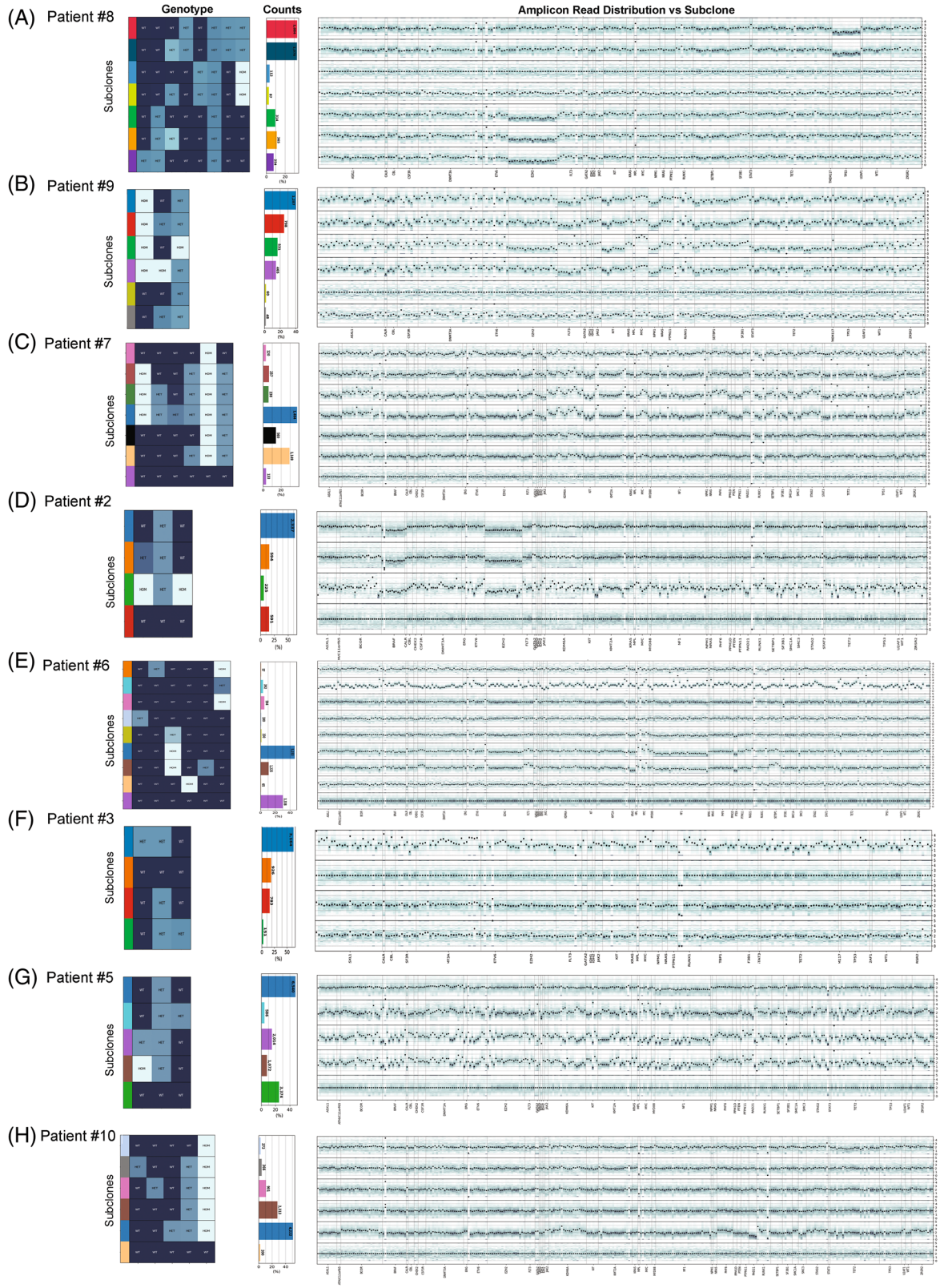

FIGURE 3 Ploidy landscape at subclones resolution. (A–H) Lineplot showing CNVs across all amplicons for each clone. On the left, subclones, identified by the SNV-based clustering method, are shown together with their genotype. In the bar plot in the central panel, the number of cells belonging to each subclone is represented. On the right, the median ploidy for each amplicon is shown.

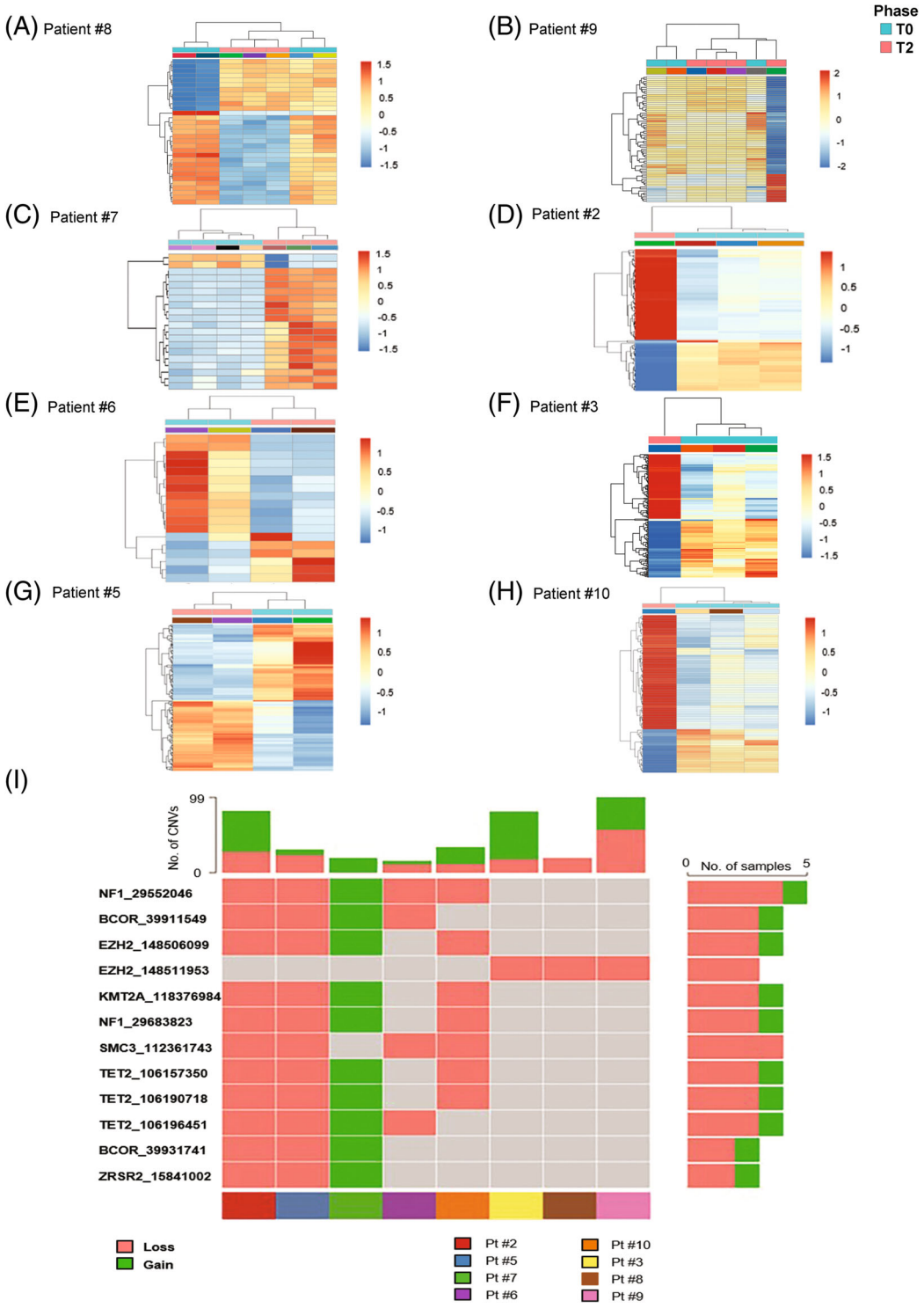

FIGURE 4 Clustering analysis based on CNV detected at subclones resolution and Copy number variants profiling in the leukemic transformation of the enrolled patients. (A–H) Heatmap of relative median ploidy values across samples, scaled by row, of amplicons significantly affected by CNVs in the comparison between BP (T2) and CP (T0). Disease-phase status and clones are shown with colored bars at the top of the heatmap. Statistical analysis based on Wilcoxon rank sum test Benjamini-Hochberg corrected test (FDR < .001, ploidy >2.5 and <−1.5) highlighted the amplicons with an altered ploidy in BP versus CP clones. Full details of the amplicons with a statistically significant altered ploidy in BP versus CP clones are reported in Table S5. (I) The waterfall plot indicates the top 12 amplicons that presented copy number variants. Each column represents individual patients. Different colors stand for different CNV types: deletions are represented in red, and amplifications are represented in green.

deregulated amplicons for each patient (for detailed description of amplicons refer to Table S5). We found that a single *NF1* amplicon was affected by CNVs in 5/5 informative patients, with copy number loss in 4 and gain in 1 patient. Other amplicons harbored recurrent CNVs in 4/5 patients; in particular, one amplicon of *SMC3* was affected by copy number loss, while *KMT2A* and *TET2* amplicons showed both copy number gain and loss (Figure 4I). Of note, *EZH2* was the gene most frequently affected by CNVs in the leukemic clones. In particular, in 7/8 patients at least one *EZH2* amplicon was affected by CNVs, in 6 cases manifesting with copy number loss (Figure 4I, Figures S5A,B and S6A,B).

We then analyzed CNVs co-occurrence/mutual exclusivity patterns. In the five patients with CNV affecting *NF1*, the abnormality co-occurred with *BRAF*, *KDM5A*, *KMT2A*, *CSF3R*, and *ETV6* CNVs. Moreover, we observed co-occurrence of gene dosage imbalances of *EZH2* and *BCOR*, two epigenetic remodelers whose loss of function was reported to have cooperating effects in leukemogenesis (Figure S7A). On the other hand, *EZH2* CNVs were mutually exclusive with *FLT3* and *MYC* aneuploidies (Figure S7B).

3.4 | Concurrent characterization of CNVs, chromatin accessibility and gene expression in BP clones by scATAC-seq and snRNA-seq analysis

SCS identified epigenetic modifier genes as the first mutational target in most instances (Figure 2). To evaluate the impact of epigenetic modifications in driving gene activation and repression during leukemic transformation, we used a multimodal approach including snRNA-seq and scATAC-seq to simultaneously study transcriptome and chromatin accessibility in $CD34^{+}$ cells from patient #8, who harbored *ASXL1*p.G646Wfs*12 as the first hit. SC CNV analysis (Figure 3A) demonstrated that the dominant $ASXL1^{mut}$ branch also harbored monoallelic *TP53* gene deletion, consistent with i(17)(q10) by conventional karyotype (Table S1), while at BP a monoallelic deletion of *EZH2* was detected in the leukemic branch (Figure 3A).

Combined snRNA-seq and scATAC-seq identified seven distinct clusters in CP and BP sample (Figure S8A,B), that were resolved in subpopulations of hematopoietic stem (HSC) and progenitor cells according to marker gene expression (Supplemental Results, Tables S6–S8 and Figure S8B). In particular, HSC and multipotent progenitors (MPP) were enriched in the BP. Moreover, two megakaryocyte erythroid progenitors (MEP) clusters were differently represented; MEP_1 cluster, displaying an erythroid bias, was enriched in CP cells, while MEP_2 cluster cells were almost exclusively found at BP (Figure S8C). Of note, leukemic cells in the MEP_2 cluster were specifically marked by deletion of *EZH2* (Figure S8D,E), as inferred by CNVs analysis of scATAC-seq data, while chromosome 17q amplification was found in a large fraction of cells both at CP and BP (Figures S9A and S8D, respectively). Overall, this finding suggested that BP was driven by a subclone harboring chromosome 7 deletion. GSEA and chromatin module activation analysis showed significant enrichment of EZH2 targets in MEP_2 cluster (Figure S8F–H), as well as increased polycomb repressive complex 2 (PRC2) and SUZ12 targets' accessibility, consistent with *EZH2* loss and mRNA reduction (Figure S9B–D).

Moreover, we found that NF-kB family transcription factors motifs were enriched in more accessible chromatin regions of BP cells with HSC phenotype, while GATA family motifs were enriched in MEP_1 cluster (see Supplemental Results, Figures S8I and S9E–H). In addition, reduced accessibility of EGR1 and EGR3 motifs was found in MEP_2 cluster cells (Figure S8J), consistent with WT1 impaired activity due to the loss-of-function *WT1*p.R467W mutation, since WT1 is involved in TET2-mediated DNA demethylation and shares its DNA binding motif with EGR family. Accordingly, a signature composed of WT1 target genes resulted negatively enriched and less active in MEP_2 cluster (Figure S8K–M), suggesting that the acquired WT1 pathogenic variant was enriched in this cluster and contributed to leukemic transformation.

4 | DISCUSSION

Owing to their intrinsic propensity of stepwise evolution from a long-course CP to BP, MPN constitute a unique model for elucidating patterns of cancer evolution and phenotype.[23,24] Past seminal studies relied on colony picking to highlight relationships between order of mutation acquisition by progenitor cells and clinical phenotype in CP,[25,26] while the study of evolutionary relationships between CP cells and leukemic blasts to elucidate the "patient's journey through cancer"[27] was hampered by intrinsic technical constrains.[28] More recent techniques for SCS generate information of unforeseen granularity regarding clonal architecture and dynamics[29–32] and also response to therapy.[21,33] By interrogating paired samples collected at CP diagnosis and BP evolution, we analyzed the evolutionary pattern of mutations and CNVs in 10 MPN patients; in one representative case, we contextually generated multimodal data sets informing also on RNA expression and chromatin accessibility.

Our results, in line with a previous report,[30] indicate an overall good comparative performance of conventional, panel-based, bulk sequencing and SCS as regards mutation identification and VAF quantification. However, bulk sequencing failed to identify low-represented variants (VAF <2%) in 40% of cases and, most importantly, clones harboring such mutations were those that predominantly expanded at BP, overtaking other clones detected at diagnosis. Thus, one might anticipate that serial analysis of clonal dynamics by SCS might allow to precociously identify the emergence and expansion of clone(s) harboring mutation(s) with leukemic potential. Studies pointed to clonal evolution as being relevant for changes in clinical phenotype in MPN.[34] Emergence of *JAK2*V617F homozygous clones in PV is associated with higher rate of transformation to postPV-myelofibrosis and thrombotic events[35–38] and to myelofibrotic transformation in ET.[36,39] However, before being able to prospectively value the changes of tumor clone asset for clinical purposes, aimed at identifying patients in need of closer monitoring and, prospectively, earlier intervention, a deeper knowledge of clonal dynamics along the MPN

natural history, also envisioning patients with decade-long uncomplicated disease, is needed.

The emergence of new dominating clone(s), known as "clonal sweep," underlined progression to MPN-BP in most instances. SCS demonstrated that the magnitude of clonal sweep was highly heterogeneous, with patterns of either predominantly monoclonal leukemia involving >75% of blasts cells in half of cases, or an oligoclonal disease with >2 clones in the remaining cases. It is also noteworthy that no patients at CP diagnosis showed only one mutated clone (whatever the mutation) variably interspersed with wild-type hematopoiesis, suggesting that the asserted monoclonal nature of MPN, coming from seminal studies on G6PDH isoenzymes[40] and erythroid colony formation,[41] should be reinterpreted as prevalently oligoclonal, thanks to granularity offered by SCS. Furthermore, in two patients we were unable to identify wild-type cells in CP sample, and phylogeny reconstruction indicated that hematopoiesis was sustained by primordial cells harboring mutations in *ASXL1* and *TET2*, followed by *CALR* mutation. This finding might be interpreted in the light of recent evidences of long latency between acquisition of driver mutation and disease manifestation,[42] resulting in progressive dominance of a clonal hematopoiesis pattern.

One limitation of the current study, and in general of SCS-based approaches, is that genomic interrogation relies on pre-selected gene panels, developed on prior knowledge of most relevant and frequent mutations in myeloid neoplasms. Therefore, in principle, one might miss what is not known a priori, as exemplified by the two cases where we were unable to detect any worthwhile change in clonal architecture from CP to BP. Indeed, we might have missed novel mutations in coding genes or variations in regulatory regions resulting in abnormal protein expression/stability, not interrogated in the predesigned gene panels. This notwithstanding, our findings point to *EZH2* as commonly involved in transition to BP, since we found CNVs in different *EZH2* amplicons in 7 out of 8 informative patients, with 6 as CN loss. *EZH2* mutations were found in 8%–10% of CP patients,[43] are associated with reduced survival[44] and included in the high molecular risk category,[3,45,46] although *EZH2* CNVs were not specifically addressed. Loss of *Ezh2* in *JAK2*V617F mice resulted in an accelerated MF phenotype.[47] Chromosome 7 loss or 7q-, involving 7q36.1 where *EZH2* is located, is associated with worse survival in AML and myelodysplastic syndrome. EZH2 may act as an oncogene or tumor-suppressor depending on cellular context.[48] In myeloid neoplasms, abnormalities at *EZH2* locus usually result in loss of function, while in germinal center-like diffuse B-cell lymphoma and follicular lymphoma gain-of-function mutations occur at EZH2 Y64.[49] Consistent with the known function of EZH2 as catalytic subunit of PRC2, promoters of *EZH2* targets resulted more accessible in MEP_2 cluster cells, that accumulated at BP in one patient and displayed chromosome 7 deletion, supporting *EZH2*-mediated transcriptional deregulation.[50]

Interpretation of SCS data allowed also to interrogate CNVs as an additional level of genetic complexity involved in evolution to MPN-BP.[51–53] By inferring CNVs of different amplicons, we found >7-fold more regions affected by CN gain or loss in BP compared to CP samples, and hierarchical clustering analysis sharply separated CP and BP clones based on CN profiles in all patients. Among most commonly affected genes, in addition to the aforementioned *EZH2*, we found *NF1*, encoding for a tumor suppressor gene mutated in 10%–15% of patients with juvenile myelomonocytic leukemia (JMML). *NF1* is usually homozygously mutated due to segmental uniparental disomy of large part of chromosome 19 or compound-heterozygous inactivating mutations,[54] and characterizes predominantly a myeloproliferative phenotype. Genes less commonly involved in CNVs were *BCOR* and *KMT2A*, both expressed in AML. However, we acknowledge that the panel-based analysis of CNVs may have missed other relevant abnormalities in genes not covered by current design.

In conclusion, in this study we have approached the cellular heterogeneity of MPN blast phase exploiting the ideal advantages offered by single-cell sequencing.[29] Results contribute to the understanding of mutation dynamics linked with clone emergence and predominance, and have highlighted the potential role of copy number variations in the process of blast evolution. Our data also point to *EZH2* as recurrently affected by mutations and CNVs in MPN-BP suggesting a pivotal role in leukemic transformation, that remains to be confirmed further. Furthermore, functional enrichment analysis considering single-nucleotide and copy number variants in blast cells highlighted networks of dysregulated pathways, among which the most prominent were signal transduction, including FLT3 signaling and MAPK, and transcriptional regulation, that might inform clues to treatment (Figure S10). Provided that further technological development results in swiftly implementation of single-cell methods in clinical laboratories, serial assessment of clonal dynamics might allow early detection of impending disease transformation and potentially translate in better therapeutic management, including target drugs and timely stem cell transplantation.

AUTHOR CONTRIBUTIONS

Paola Guglielmelli, Alessandro Maria Vannucchi, and Rossella Manfredini designed the research, analyzed data, and drafted the manuscript. Laura Calabresi, Chiara Carretta, Simone Romagnoli, Giada Rotunno, Sandra Parenti, Matteo Bertesi, Niccolò Bartalucci, Sebastiano Rontauroli, Chiara Chiereghin, Sara Castellano, Chiara Maccari, and Fiorenza Vanderwert performed research and contributed to data analysis. Francesco Mannelli, Matteo Della Porta, Paola Guglielmelli and Alessandro Maria Vannucchi contributed patient samples and clinical data. All authors contributed to writing the report, and approved the final submitted version.

FUNDING INFORMATION

This project was supported by grants from Associazione Italiana per la Ricerca sul Cancro-AIRC, project 5 per Mille MYNERVA (MYeloid NEoplasms Research Venture AIRC), code 21267; AIRC IG project 19818; The "EDITOR," Accelerator Award project funded through a partnership between Cancer Research UK, Fondazione AIRC and Fundación Científica de la Asociacion Española Contra el Cáncer. Also supported by Italian Ministry of Health, project Ricerca Finalizzata, code NET-2018-12365935. The work was supported also by

generous donation from Famiglia Olmetti/Minguzzi and Associazione Italiana per le Leucemie, Firenze.

CONFLICT OF INTEREST STATEMENT

There is no conflict of interest to declare from any of the authors.

DATA AVAILABILITY STATEMENT

Single-cell DNA sequencing data, BioProject and BioSample, are available via the NCBI Sequence Read Archive with accession: PRJNA911024. scATAC-seq+snRNA-seq sequencing data are available via NCBI Gene Expression Omnibus repository, accession: GSE221946.

ORCID

Chiara Carretta https://orcid.org/0000-0001-5952-0818
Niccolò Bartalucci https://orcid.org/0000-0002-9328-3948
Sebastiano Rontauroli https://orcid.org/0000-0003-2496-4181
Francesco Mannelli https://orcid.org/0000-0003-4810-6501
Alessandro Maria Vannucchi https://orcid.org/0000-0001-5755-0730

REFERENCES

1. Arber DA, Orazi A, Hasserjian RP, et al. International consensus classification of myeloid neoplasms and acute leukemias: integrating morphologic, clinical, and genomic data. *Blood*. 2022;140(11):1200-1228.
2. Al-Ghamdi YA, Lake J, Bagg A, et al. Triple-negative primary myelofibrosis: a bone marrow pathology group study. *Mod Pathol*. 2023;36(3):100016.
3. Vannucchi AM, Lasho TL, Guglielmelli P, et al. Mutations and prognosis in primary myelofibrosis. *Leukemia*. 2013;27(9):1861-1869.
4. Tefferi A, Lasho T, Finke C, et al. Targeted deep sequencing in primary myelofibrosis. *Blood Adv*. 2016;1:105-111.
5. Tefferi A, Lasho T, Guglielmelli P, et al. Targeted deep sequencing in polycythemia vera and essential thrombocythemia. *Bloood Adv*. 2016;1:21-30.
6. Duncavage EJ, Bagg A, Hasserjian RP, et al. Genomic profiling for clinical decision making in myeloid neoplasms and acute leukemia. *Blood*. 2022;140(21):2228-2247.
7. Mesa RA, Verstovsek S, Cervantes F, et al. Primary myelofibrosis (PMF), post polycythemia vera myelofibrosis (post-PV MF), post essential thrombocythemia myelofibrosis (post-ET MF), blast phase PMF (PMF-BP): consensus on terminology by the international working group for myelofibrosis research and treatment (IWG-MRT). *Leuk Res*. 2007;31:737-740.
8. Dunbar AJ, Rampal RK, Levine R. Leukemia secondary to myeloproliferative neoplasms. *Blood*. 2020;136(1):61-70.
9. Mascarenhas J. A concise update on risk factors, therapy, and outcome of leukemic transformation of myeloproliferative neoplasms. *Clin Lymphoma Myeloma Leuk*. 2016;16(Suppl):S124-S129.
10. Tefferi A, Mudireddy M, Mannelli F, et al. Blast phase myeloproliferative neoplasm: Mayo-AGIMM study of 410 patients from two separate cohorts. *Leukemia*. 2018;32(5):1200-1210.
11. Gangat N, Guglielmelli P, Szuber N, et al. Venetoclax with azacitidine or decitabine in blast-phase myeloproliferative neoplasm: a multicenter series of 32 consecutive cases. *Am J Hematol*. 2021;96(7):781-789.
12. Tefferi A, Bacigalup A. Blast phase myeloproliferative neoplasm: transplant to the rescue. *Am J Hematol*. 2023;98:553-555.
13. Lasho TL, Mudireddy M, Finke CM, et al. Targeted next-generation sequencing in blast phase myeloproliferative neoplasms. *Blood Adv*. 2018;2(4):370-380.
14. Milosevic JD, Puda A, Malcovati L, et al. Clinical significance of genetic aberrations in secondary acute myeloid leukemia. *Am J Hematol*. 2012;87:1010-1016.
15. Green A, Beer P. Somatic mutations of IDH1 and IDH2 in the leukemic transformation of myeloproliferative neoplasms. *N Engl J Med*. 2010;362(4):369-370.
16. Marcellino BK, Hoffman R, Tripodi J, et al. Advanced forms of MPNs are accompanied by chromosomal abnormalities that lead to dysregulation of TP53. *Blood Adv*. 2018;2(24):3581-3589.
17. Beer PA, Delhommeau F, LeCouedic JP, et al. Two routes to leukemic transformation after a JAK2 mutation-positive myeloproliferative neoplasm. *Blood*. 2010;115(14):2891-2900.
18. Beer PA, Ortmann CA, Stegelmann F, et al. Molecular mechanisms associated with leukaemic transformation of MPL-mutant myeloproliferative neoplasms. *Haematologica*. 2010;95(12):2153-2156.
19. Parenti S, Rontauroli S, Carretta C, et al. Mutated clones driving leukemic transformation are already detectable at the single-cell level in CD34-positive cells in the chronic phase of primary myelofibrosis. *NPJ Precis Oncol*. 2021;5(1):4.
20. Saliba AN, Gangat N. Accelerated and blast phase myeloproliferative neoplasms. *Best Pract Res Clin Haematol*. 2022;35(2):101379.
21. Tong J, Sun T, Ma S, et al. Hematopoietic stem cell heterogeneity is linked to the initiation and therapeutic response of myeloproliferative neoplasms. *Cell Stem Cell*. 2021;28(3):502-513.e506.
22. Rontauroli S, Castellano S, Guglielmelli P, et al. Gene expression profile correlates with molecular and clinical features in patients with myelofibrosis. *Blood Adv*. 2021;5(5):1452-1462.
23. Maslah N, Benajiba L, Giraudier S, Kiladjian JJ, Cassinat B. Clonal architecture evolution in myeloproliferative neoplasms: from a driver mutation to a complex heterogeneous mutational and phenotypic landscape. *Leukemia*. 2023;37:957-963.
24. Rolles B, Mullally A. Molecular pathogenesis of myeloproliferative neoplasms. *Curr Hematol Malig Rep*. 2022;17(6):319-329.
25. Ortmann CA, Kent DG, Nangalia J, et al. Effect of mutation order on myeloproliferative neoplasms. *N Engl J Med*. 2015;372:601-612.
26. Nangalia J, Nice FL, Wedge DCD, et al. DNMT3A mutations occur early or late in patients with myeloproliferative neoplasms and mutation order influences phenotype. *Haematologica*. 2015;100:e438-e442.
27. Nangalia J, Campbell PJ. Genome sequencing during a patient's journey through cancer. *N Engl J Med*. 2019;381(22):2145-2156.
28. Nangalia J, Mitchell E, Green AR. Clonal approaches to understanding the impact of mutations on hematologic disease development. *Blood*. 2019;133(13):1436-1445.
29. O'Sullivan JM, Mead AJ, Psaila B. Single-cell methods in myeloproliferative neoplasms: old questions, new technologies. *Blood*. 2023;141(4):380-390.
30. Miles LA, Bowman RL, Merlinsky TR, et al. Single-cell mutation analysis of clonal evolution in myeloid malignancies. *Nature*. 2020;587(7834):477-482.
31. Ediriwickrema A, Gentles AJ, Majeti R. Single-cell genomics in AML: extending the frontiers of AML research. *Blood*. 2023;141(4):345-355.
32. Morita K, Wang F, Jahn K, et al. Clonal evolution of acute myeloid leukemia revealed by high-throughput single-cell genomics. *Nat Commun*. 2020;11(1):5327.
33. Naldini MM, Casirati G, Barcella M, et al. Longitudinal single-cell profiling of chemotherapy response in acute myeloid leukemia. *Nat Commun*. 2023;14(1):1285.
34. Moliterno AR, Kaizer H, Reeves BN. JAK2V617F allele burden in polycythemia vera: burden of proof. *Blood*. 2023;141:1934-1942.
35. Vannucchi AM, Antonioli E, Guglielmelli P, et al. Prospective identification of high-risk polycythemia vera patients based on JAK2V617F allele burden. *Leukemia*. 2007;21(9):1952-1959.
36. Vannucchi AM, Antonioli E, Guglielmelli P, et al. Clinical profile of homozygous JAK2V617F mutation in patients with polycythemia vera or essential thrombocythemia. *Blood*. 2007;110:840-846.

37. Passamonti F, Rumi E, Pietra D, et al. A prospective study of 338 patients with polycythemia vera: the impact of JAK2 (V617F) allele burden and leukocytosis on fibrotic or leukemic disease transformation and vascular complications. *Leukemia*. 2010;24:1574-1579.
38. Guglielmelli P, Loscocco GG, Mannarelli C, et al. JAK2V617F variant allele frequency >50% identifies patients with polycythemia vera at high risk for venous thrombosis. *Blood Cancer J*. 2021;11(12):199.
39. Loscocco GG, Guglielmelli P, Gangat N, et al. Clinical and molecular predictors of fibrotic progression in essential thrombocythemia: a multicenter study involving 1607 patients. *Am J Hematol*. 2021;96(11):1472-1480.
40. Adamson JW, Fialkow PJ, Murphy S, Prchal JF, Steinmann L. Polycythemia vera: stem-cell and probable clonal origin of the disease. *N Engl J Med*. 1976;295(17):913-916.
41. Prchal JF, Axelrad AA. Letter: bone-marrow responses in polycythemia vera. *N Engl J Med*. 1974;290(24):1382.
42. Sousos N, Ní Leathlobhair M, Simoglou Karali C, et al. In utero origin of myelofibrosis presenting in adult monozygotic twins. *Nat Med*. 2022;28(6):1207-1211.
43. Ernst T, Chase AJ, Score J, et al. Inactivating mutations of the histone methyltransferase gene EZH2 in myeloid disorders. *Nat Genet*. 2010;42(8):722-726.
44. Guglielmelli P, Biamonte F, Score J, et al. EZH2 mutational status predicts poor survival in myelofibrosis. *Blood*. 2011;118(19):5227-5234.
45. Guglielmelli P, Lasho TL, Rotunno G, et al. MIPSS70: mutation-enhanced international prognostic score system for transplantation-age patients with primary myelofibrosis. *J Clin Oncol*. 2018;36(4):301-318.
46. Tefferi A, Guglielmelli P, Lasho TL, et al. MIPSS70+ version 2.0: mutation and karyotype-enhanced international prognostic scoring system for primary myelofibrosis. *J Clin Oncol*. 2018;36:1769-1770.
47. Shimizu T, Kubovcakova L, Nienhold R, et al. Loss of Ezh2 synergizes with JAK2-V617F in initiating myeloproliferative neoplasms and promoting myelofibrosis. *J Exp Med*. 2016;213(8):1479-1496.
48. Rinke J, Chase A, Cross NCP, Hochhaus A, Ernst T. EZH2 in myeloid malignancies. *Cell*. 2020;9(7):1639.
49. Morin RD, Johnson NA, Severson TM, et al. Somatic mutations altering EZH2 (Tyr641) in follicular and diffuse large B-cell lymphomas of germinal-center origin. *Nat Genet*. 2010;42:181-185.
50. Blackledge NP, Klose RJ. The molecular principles of gene regulation by polycomb repressive complexes. *Nat Rev Mol Cell Biol*. 2021;22(12):815-833.
51. Alkan C, Coe BP, Eichler EE. Genome structural variation discovery and genotyping. *Nat Rev Genet*. 2011;12(5):363-376.
52. Chaisson MJ, Wilson RK, Eichler EE. Genetic variation and the de novo assembly of human genomes. *Nat Rev Genet*. 2015;16(11):627-640.
53. Yi K, Ju YS. Patterns and mechanisms of structural variations in human cancer. *Exp Mol Med*. 2018;50(8):1-11.
54. Stephens K, Weaver M, Leppig KA, et al. Interstitial uniparental isodisomy at clustered breakpoint intervals is a frequent mechanism of NF1 inactivation in myeloid malignancies. *Blood*. 2006;108(5):1684-1689.

SUPPORTING INFORMATION

Additional supporting information can be found online in the Supporting Information section at the end of this article.

How to cite this article: Calabresi L, Carretta C, Romagnoli S, et al. Clonal dynamics and copy number variants by single-cell analysis in leukemic evolution of myeloproliferative neoplasms. *Am J Hematol*. 2023;98(10):1520-1531. doi:10.1002/ajh.27013